Vol. 28 • No. 30 • July 25 • 2018

www.afm-journal.de

ADVANCED FUNCTIONAL MATERIALS

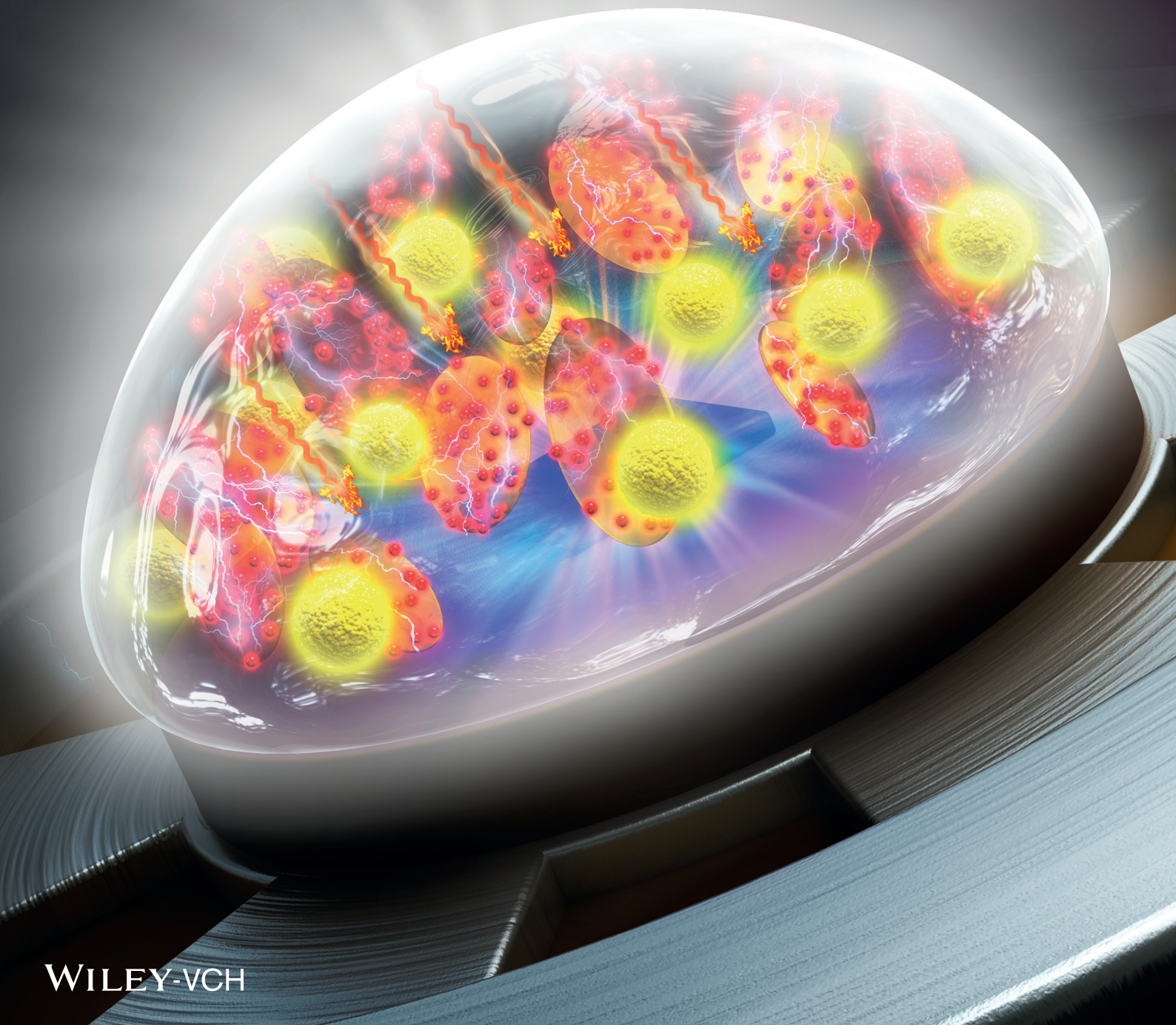

WILEY-VCH

ADVANCED FUNCTIONAL MATERIALS
www.afm-journal.de

Targeting Cooling for Quantum Dots in White QDs-LEDs by Hexagonal Boron Nitride Platelets with Electrostatic Bonding

Bin Xie, Haochen Liu, Run Hu, Chaofan Wang, Junjie Hao, Kai Wang, and Xiaobing Luo**

Although quantum dots (QDs) show excellent advantages in flexible wavelength-tuning and high color rendering capability in white light-emitting diodes (WLEDs) lighting and display applications, the less-than-one quantum efficiency inevitably gives rise to a non-negligible heat generation problem, which induces high-temperature quenching issues of QDs and severely hinders their potential applications. Efficient heat dissipation for these nanoscale QDs is challenging since these nanoparticle "heat sources" are usually embedded in a low-thermal conductivity polymer matrix. In this work, this problem is attempted by targeting cooling of the QDs in the silicone matrix by electrostatically bonding the hexagonal boron nitride (hBN) platelets onto QDs without sacrificing the optical performance of WLEDs. The red-emissive QDs/hBN composites are mixed with yellow-emissive phosphor to fabricate QDs/hBN-WLEDs. Due to the effective heat transfer channels established by the QDs/hBN in the silicone, the heat could be dissipated efficiently to ambient air, and the working temperature of WLEDs is reduced by 22.7 °C at 300 mA. The QDs/hBN-WLEDs still maintain a high luminous efficiency of 108.5 lm W^{-1} and a high color rendering index of Ra > 95, R9 > 90, showing that the present strategy can improve heat dissipation without sacrificing the optical performance.

1. Introduction

Over the past two decades, colloidal quantum dots (QDs) have received widespread attention in many applications, such as light-emitting diodes (LEDs), solar cells, and biosensors[1–3] due to their unique optical properties compared with traditional inorganic phosphors and organic dyes, including narrow and size-tunable emission spectra, broad absorption spectra, and high quantum efficiency.[4–6] QDs have been considered promising alternatives for next-generation high-performance lighting and display devices.[7,8] It has been demonstrated previously that adding red-emissive QDs into conventional phosphor-converted LEDs could greatly enhance their color rendering index,[9,10] which provides a facile way toward high-quality white LEDs (WLEDs). However, the practical application of QDs in WLEDs has been severely hindered due to the LEDs packaging issue in which QDs and phosphor are mixed with silicone gel. One major reason is that QDs are sensitive to ambient environment and temperature, leading to considerable thermal quenching and degradation.[11,12] Cooling the nanoscale QDs is challenging since these nanoparticle "heat sources" are usually embedded in low-thermal conductivity polymer matrix. Possible solutions have been achieved by embedding QDs in polymer matrices or growing inorganic barrier layers like silicon and alumina.[13–16] Whereas, these methods have to employ complicated QDs surface-treatment processes, and the thick barrier layers usually cause partial degradation of optical performance, making them less economically suitable for WLEDs applications.

Compared with modifying QDs surface properties, reducing QDs' working temperature seems to be more applicable to solve the QDs thermal quenching problem. Generally, this can be realized by incorporating high-thermal conductivity fillers into silicone gel, thus reinforcing the thermal conductivity of QDs/phosphor silicone gel, and consequently enhance the heat dissipation from silicone gel to ambient air. The reinforcing fillers should be highly thermal-conductive, as well as optically transparent with negligible light absorption. Nevertheless, most of reinforcing fillers such as graphene, carbon nanotube, and metals are light-absorbing materials, leading to serious optical energy loss.[17–19] Poostforush and Azizi mixed crystallized anodic aluminum oxide with epoxy resin at 39 vol% filler loading, and the obtained composite had a through-plane thermal conductivity of 1.13 W (m K)$^{-1}$ and a transparency of 72% that of pure epoxy.[20] Patel et al. utilized alumina powders to enhance the thermal conductivity of polymethyl methacrylate (PMMA) to 0.233 W (m K)$^{-1}$, while the transmittance was decreased by ≈10% than the neat matrix polymer at a filler content of only 0.5 wt%.[21] For these fillers, there is a trade-off between the transparency and the thermal conductivity even at low loadings, and it seems difficult to achieve both properties simultaneously.

Recently, hexagonal boron nitride (hBN) has attracted significant attention as a new reinforcing filler due to its high thermal

B. Xie, Prof. R. Hu, C. Wang, Prof. X. Luo
State Key Laboratory of Coal Combustion
School of Energy and Power Engineering
Huazhong University of Science and Technology
Wuhan 430074, China
E-mail: luoxb@hust.edu.cn
H. Liu, J. Hao, Prof. K. Wang
Department of Electrical and Electronic Engineering
Southern University of Science and Technology
Shenzhen 518055, China
E-mail: wangk@sustc.edu.cn
The ORCID identification number(s) for the author(s) of this article can be found under https://doi.org/10.1002/adfm.201801407.

DOI: 10.1002/adfm.201801407

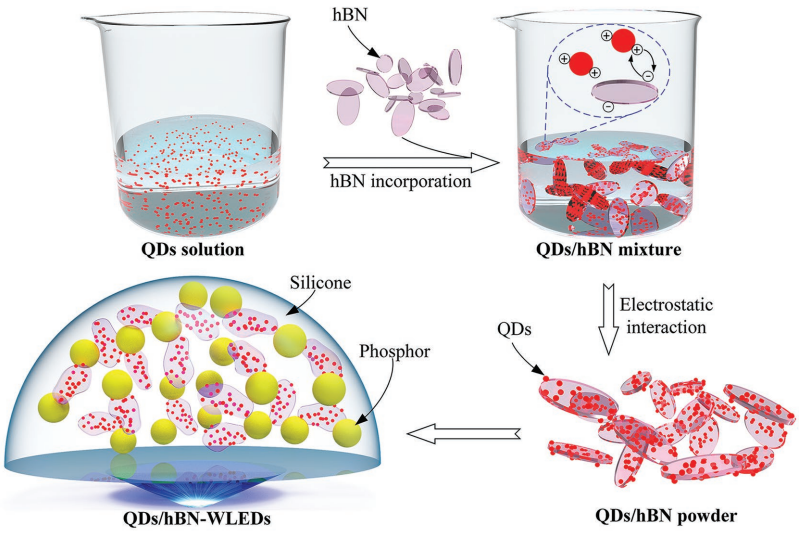

Figure 1. Schematic showing the preparation of QDs/hBN composites and the fabrication of QDs/hBN-WLEDs.

conductivity (≈300 W m^{-1} K^{-1}) and electrically insulating properties.[22–24] More importantly, the hBN platelets are white powder with negligible light absorption (as we test hereinafter), which seems promising as suitable filler candidate in QDs. Moreover, simply adding/embedding hBN platelets into QDs/phosphor silicone is not enough to remove the heat from QDs. We have to build effective physical/chemical interaction between QDs and hBN platelets so that the heat generation of targeting QDs can be dissipated effectively.

In this work, the highly thermal-conductive and luminescent QDs/hBN composites were prepared by coating QDs onto hBN surface through the electrostatic interaction. Then the red-emissive QDs/hBN composites were mixed with yellow-emissive phosphor to fabricate QDs/hBN-WLEDs, as depicted in **Figure 1**. Both the optical and thermal characteristics of QDs/hBN-WLEDs were measured with comparison with the QDs-WLEDs without hBN. Compared with the QDs-WLEDs, the working temperature of QDs/hBN-WLEDs was reduced by 22.7 °C at 300 mA, while the luminous efficiency and color rendering index can be maintained as high as 108.5 lm W^{-1}, Ra > 95 and R9 > 90. The present strategy can improve heat dissipation without sacrificing the optical performance, which shows the practical feasibility in the package-inside thermal management.

2. Results and Discussion

Figure 2a,b) displays the photographs of the QDs solution, hBN platelets, and QDs/hBN composites under daylight and UV light irradiation. It can be seen that under daylight, the hBN platelets show pure white color with less light absorption, and the QDs/hBN composites are yellowish powder. Under UV light, both the QDs solution and QDs/hBN composites show bright red emission, indicating that the incorporation of hBN platelets did not cause significant efficiency drop toward QDs. Figure 2c provides the photoluminescence (PL) spectra of the QDs solution and QDs/hBN platelets. The peak wavelength and full-width-at-half-maximum (FWHM) of the QDs solution were measured as 625 and 34.5 nm, respectively. After incorporated with hBN platelets, QDs' peak wavelength and FWHM changed to 626 and 35 nm, which means that the incorporation process has less effect to QDs spectral properties. The slight redshift of peak wavelength is attributed to the quantum states

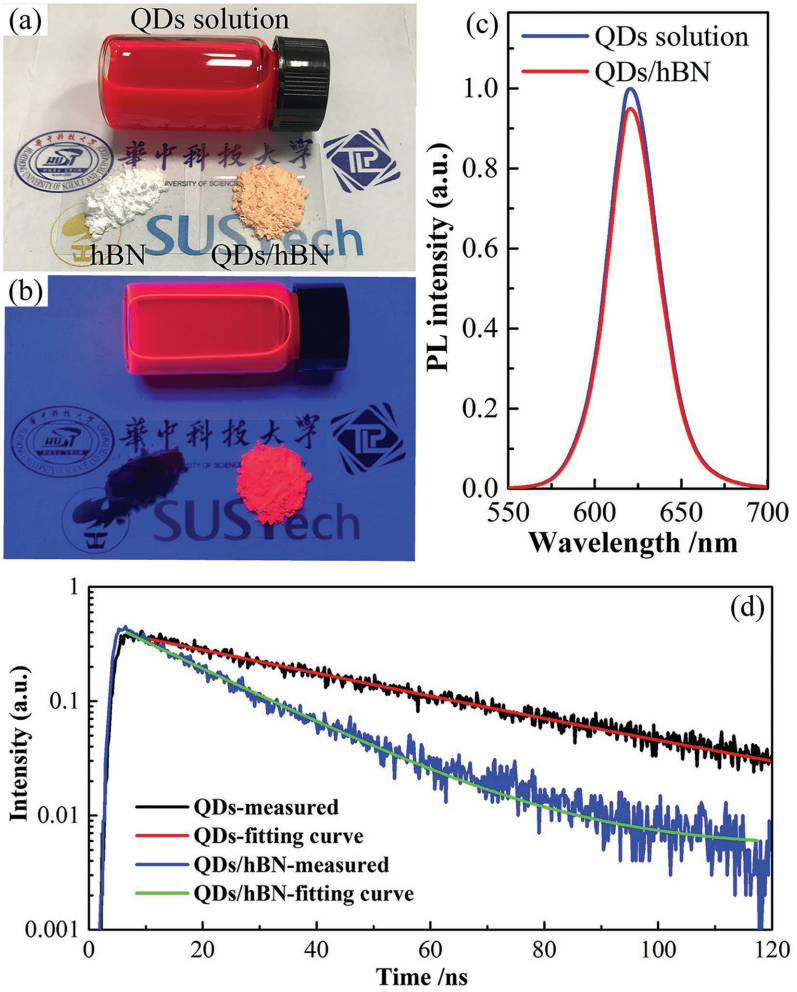

Figure 2. Photographs of the QDs solution, hBN and QDs/hBN composites under a) daylight and b) UV light irradiation. c) PL spectra of the QDs solution and QDs/hBN composites. d) TRPL decay curves of the QDs and QDs/hBN composites.

Table 1. Values for TRPL characteristics of CdSe/ZnS QDs and QDs/hBN composites.

Sample	$\tau 1$	A_1
CdSe/ZnS QDs	41.9	357.127
QDs/hBN composites	18.1	398.347

overlapping effect among closed QDs, which because the physical separations among QDs become smaller during the incorporation process.[9] The PL quantum yield (QY) decreased from 82% to 74% after incorporating QDs onto hBN surface. To further investigate the underlying origins of QY decrease, the time-resolved PL (TRPL) spectra of both CdSe/ZnS QDs and QDs/hBN samples were measured in air, and the decay curves were depicted in Figure 2d. These decay curves can be well fitted by an exponential function $I(t) = A_1 e^{-t/\tau 1}$ where $I(t)$ is the PL initial intensity at time t. The fitting parameters A_1 and PL lifetime are listed in **Table 1**. The PL lifetime of CdSe/ZnS QDs is calculated as 41.9 ns, and that of QDs/hBN composites is 18.1 ns. The reduction of PL QY can be explained by the energy transfer process took place from QDs donors to hBN acceptors or adjacent QDs acceptors because energy transfer process is an additional nonradiative de-excitation path.

Figure 3a shows the high resolution transmission electron microscope (HRTEM) images of CdSe/ZnS core–shell QDs in different resolutions, respectively. The measured nanoparticles demonstrate uniform size distribution and clear lattice fringes that suggests monodispersed QDs with good crystallinity. The average size of QDs was measured as 6.8 nm. Figure 3b,c displays the scanning electron microscope (SEM) images of hBN platelets and QDs/hBN composites, respectively. The SEM characterization reveals that the diameter of hBN platelets ranges from ≈6 to ≈20 µm, and the size distribution of platelets changes very little during the QDs incorporation process. Further, the energy dispersive spectroscopy (EDS) analysis of QDs/hBN composites was conducted. The results reveal the presence of 32.1 at% boron, 36.2 at% nitrogen, 0.14 at% cadmium, and 0.21 at% zinc. Moreover, the elemental mapping by EDS shows a uniform distribution of QDs, and no large agglomerate of nanoparticles is observed in Figure 3d. To further observe the distribution of QDs on hBN platelets, scanning TEM (STEM) image of QDs/hBN composites was measured and displayed in Figure 3e. The clear lattice fringes of both hBN and QDs demonstrate the desired QDs-on-hBN structure. Figure 3f shows the high-angle-annular-dark-field STEM (HAADF-STEM) image of QDs/hBN composites, from which we can directly observe the uniform distribution of QDs

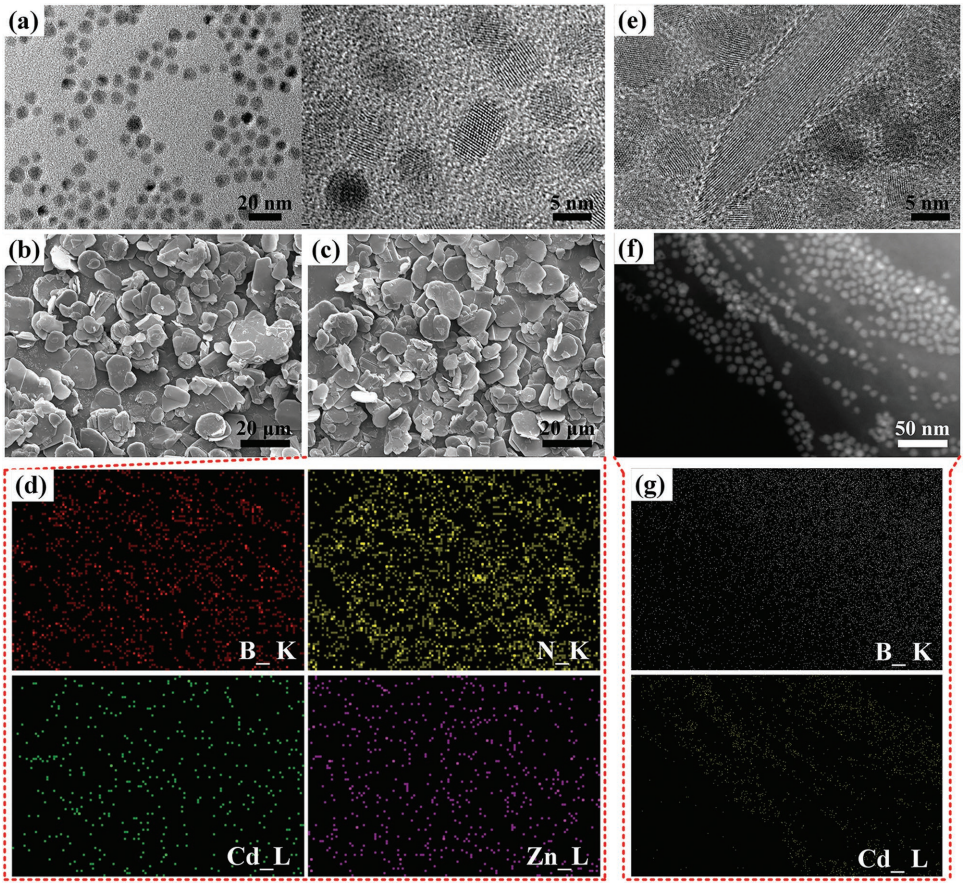

Figure 3. a) HRTEM images of the QDs solution. b) SEM image of the hBN platelets. c) SEM image of the QDs/hBN composites. d) Elemental mapping images of the QDs/hBN composites collected from the same location of (c). e) STEM image of the QDs/hBN composites. f) HAADF-STEM image of the QDs/hBN composites. g) Elemental mapping images of the QDs/hBN composites collected from the same location of (f).

on hBN platelets without agglomeration. Figure 3g shows the EDS mapping images of boron and cadmium collected from the same location of Figure 3f. To investigate the effectiveness of QDs-on-hBN bonding structure, 0.5 g of QDs/hBN composites were redispersed in 3 mL of chloroform and stand for 1 h. Then the supernatant chloroform was collected separately from the QDs/hBN composites. As shown in Figure S1 (Supporting Information), under UV light irradiation, the QDs/hBN composites show bright red emission while the supernatant chloroform is colorless, indicating that the effective bonding of QDs and hBN platelets was built.

In order to study the optical properties of QDs/hBN composites, both QDs- and QDs/hBN-WLEDs samples were fabricated, and their correlated color temperature (CCT) were controlled to around 4300 K (neutral white color) by fine-tuning the gel volume. It is noted that the viscosity is a critical mechanical property for the mixed gel since it directly influences the gel geometry in the fabrication of WLEDs. We have measured the viscosity of phosphor silicone gel and phosphor-QDs/hBN silicone gel under different temperature, and the results are displayed in Figure S2 (Supporting Information). It was found that the viscosity of the gel varies little (less than 0.3 Pa·s above 40 °C) after the incorporation of QDs/hBN. Therefore, the addition of QDs/hBN composites has negligible influence on the viscosity. **Figure 4**a provides the spectra and optical properties of these WLEDs samples under driving current of 20 mA. It

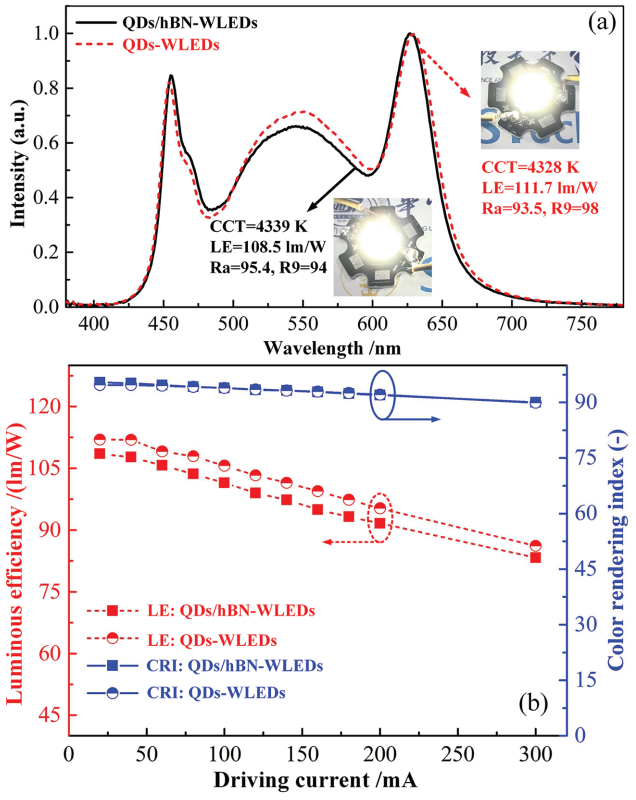

Figure 4. a) Spectral distribution and optical properties of the QDs- and QDs/hBN-WLEDs under driving current of 20 mA. b) LE and CRI of the QDs- and QDs/hBN-WLEDs under different driving currents from 20 to 300 mA.

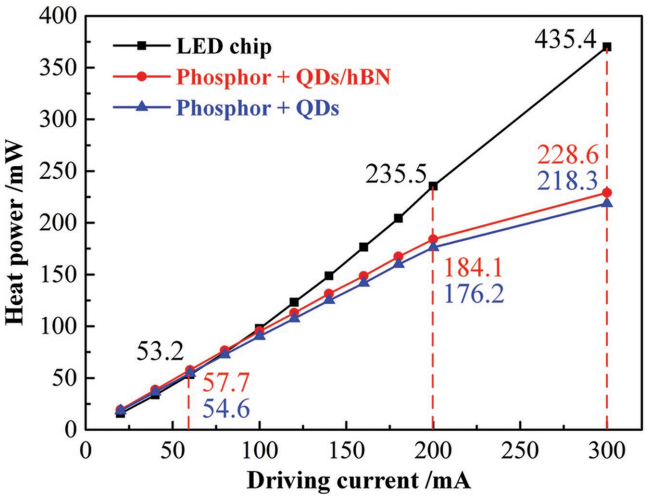

Figure 5. Measured heat generation in LED chip, QDs/hBN-phosphor layer, and QDs-phosphor layer under different driving current.

is seen that under similar spectral distribution, both WLEDs demonstrate high color rendering index (CRI) of Ra > 93 and R9 > 90, which is the rendering index for deep red color. Meanwhile, the QDs-WLEDs present high luminous efficiency (LE) of 111.7 lm W^{-1}, and that of QDs/hBN-WLEDs is 108.5 lm W^{-1}. Figure 4b shows the CRI and LE variation with increasing driving currents from 20 to 300 mA. The results suggest that the CRI of both WLEDs remain stable against increasing driving current, indicating their stable spectral distribution under different lighting conditions. The LE of both WLEDs shows similar decreasing trend under increasing driving current. This is mainly attributed to the efficiency drop of LED chip itself. Therefore, the utilization of QDs/hBN does not cause evident LE drop of WLEDs. Moreover, the QDs/hBN-WLEDs present the same optical performance and current stability as the QDs-WLEDs.

To further investigate the thermal differences between the QDs/hBN-WLEDs and QDs-WLEDs, the heat power generated in LED chip, QDs/hBN-phosphor layer, and QDs-phosphor layer were first measured and calculated according to Eqs. (1)–(3), as illustrated in **Figure 5**. The results reveal that

Table 2. Thickness and thermal conductivity used for thermal simulation.

Component	Thickness [mm]	κ [Wm^{-1} K^{-1}]
PCB metalcore	0.98	170
Thermal grease	0.05	5
Heat sink	6	170
Solder	0.05	5
LED chip	0.1	65.6
Leadframe	6	0.36
QDs-phosphor gel	1.5	0.18
QDs/hBN-phosphor gel	1.5	0.27
PCB dielectric	0.02	0.2

the heat power of LED chip is much larger than that of others, especially under large driving current. This is attributed to different kinds of nonradiative recombinations and other causes of photon annihilation occur within LED chip.[2] The heat generation in QDs/hBN-phosphor is close to that in QDs-phosphor, and their heat power increase with the increasing driving current. For instance, under 300 mA illumination, the heat power of QDs/hBN-phosphor layer and QDs-phosphor layer is 228.6 and 218.3 mW, respectively, while the heat power of LED chip is nearly twice that of QDs/hBN-phosphor layer. Table S1 (Supporting Information) lists the optical power and brightness data of bare LED module, QDs-WLEDs, and QDs/hBN-WLEDs under different driving currents.

Then, the thermal conductivity κ of QDs/hBN-phosphor gel and QDs-phosphor gel were measured by the method described in the Experimental Section. The α, C_p, and ρ of QDs-phosphor gel at 25 °C is measured as 0.098 mm^2 s^{-1}, 1.504 J (g K)$^{-1}$, and 1.22 g cm^{-3}, respectively, and those of QDs/hBN-phosphor gel was measured as 0.136 mm^2 s^{-1}, 1.568 J (g K) $^{-1}$, and 1.26 g cm^{-3}, respectively. Consequently, the κ of QDs-phosphor gel and QDs/hBN-phosphor gel was calculated as 0.18 W (m K)$^{-1}$ and 0.27 W (m K)$^{-1}$, respectively. The higher κ of QDs/hBN-phosphor gel is owing to the formation of efficient thermal pathways made by the hBN platelets. In this case, the thermal conductivity was enhanced by 50% with a weight fraction of 4.3% (volume fraction of about 2%) hBN platelets. The temperature-dependent κ data from 25 to 125 °C was also measured and displayed in Figure S3 (Supporting Information). It was found that the κ of both gels decrease slightly with the increasing testing temperature. For instance, the κ of QDs-phosphor gel and QDs/hBN-phosphor gel was calculated as 0.173 and 0.25 W (m K)$^{-1}$, respectively at 125 °C. Despite of this slight drop, the thermal conductivity was still enhanced effectively by 45%. Additionally, we also measured the thermal conductivity of QDs/hBN-phosphor gel with a higher weight fraction of 8.6% hBN platelets, and the κ was enhanced significantly by 88.9% (from 0.18 to 0.34 W (m K)$^{-1}$). While, the LE was decreased from 111.7 to 97 lm W^{-1} due to the overload of hBN platelets which interrupt the light output from QDs/hBN-phosphor gel. Therefore, it is validated that the utilization of QDs/hBN is an effective way to reinforce the thermal conductivity of phosphor gel, and the percentage of hBN platelets should be optimized to balance the heat dissipation and light output.

The thickness and thermal conductivity of each component used for thermal simulation was listed in **Table 2**. **Figure 6** gives the simulated temperature fields of two WLEDs under driving currents of 60, 200, and 300 mA. It is seen that the highest temperature of all these WLEDs are located in the top surface of silicone gel. This is mainly attributed to the relatively low thermal conductivity of silicone gel that is incapable of dissipating the heat quickly.[25,26] Under the same driving current, the highest temperature in QDs/hBN-WLEDs is lower than that in QDs-WLEDs, and the temperature reduction is more apparent at larger driving current. For instance, the temperature reduction is 5, 16.3, and 20.1 °C at 60, 200, and 300 mA, respectively. The simulation results clearly show the effectiveness of QDs/hBN on the reinforcement of heat dissipation and temperature reduction.

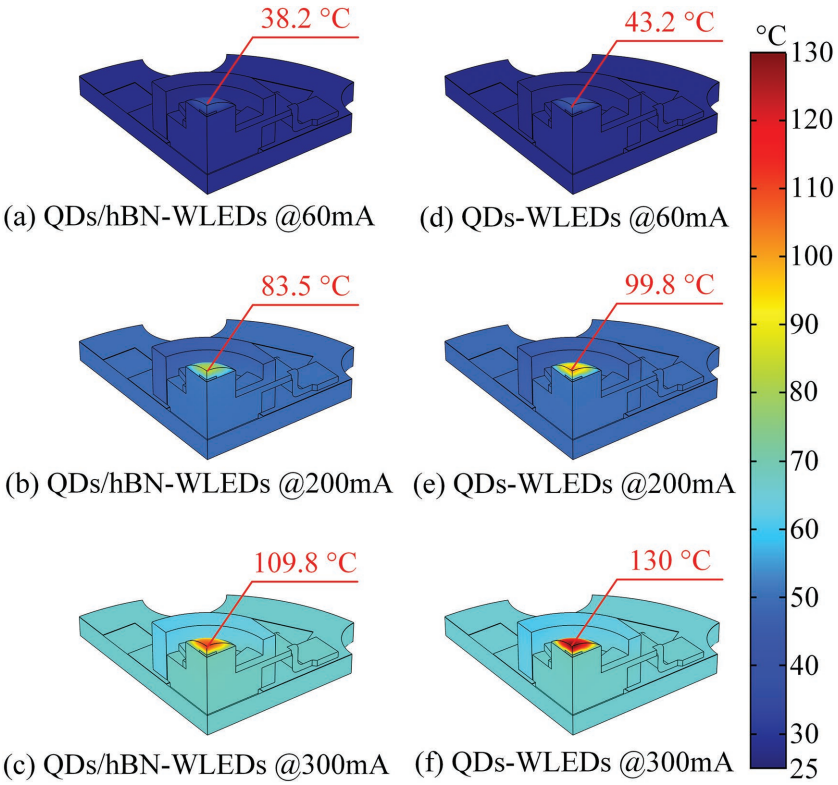

Figure 6. a–f) Simulated steady-state temperature fields of the two WLEDs under driving currents of 60, 200, and 300 mA.

To further validate our simulation results, the surface temperature distribution of the two WLEDs were measured. The QDs/hBN-WLEDs and QDs-WLEDs were connected by a series circuit so that their driving current are the same, as displayed in **Figure 7**a. The surface emissivity of QDs/hBN-phosphor gel and QDs-phosphor gel is set as 0.96.[27] The distance between camera lens and WLEDs is 0.3 m. Figure 7b,d provides the measured steady-state temperature fields at 60, 200, and 300 mA, respectively. It is seen that the simulated temperature distributions between these two WLEDs are in well accordance to the measured results, and the maximum relative deviation of the highest temperature between experimental and simulated results is 12.8% (QDs-WLEDs at 60 mA) which is within the acceptable level. The measured results demonstrate that a 22.7 °C of temperature reduction could be reached at 300 mA by the use of QDs/hBN composites. Thus, both simulated and experimental results show that the use of QDs/hBN can significantly enhance the heat dissipation and temperature reduction of WLEDs. As a result, the thermal quenching of QDs should

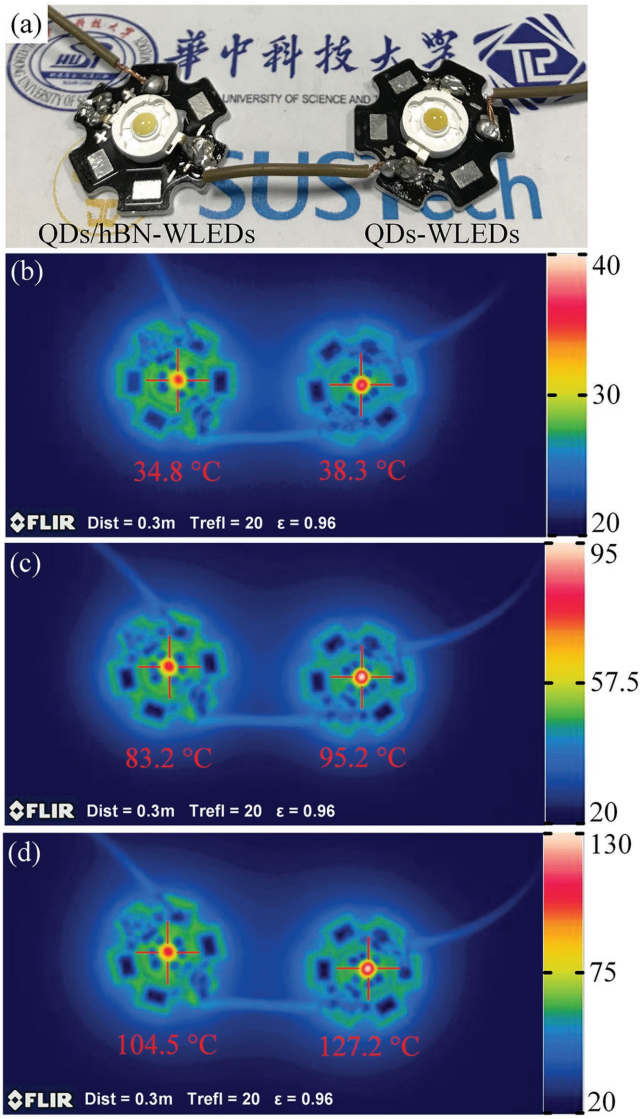

Figure 7. a) Photograph of the QDs/hBN-WLEDs and QDs-WLEDs in a series circuit. (b), (c), and (d) show the measured temperature fields at 60, 200, and 300 mA, respectively.

also be reduced by the use of QDs/hBN. Therefore, QDs-LEDs consist of blue LED chip and QDs silicone gel, and QDs/hBN-LEDs consist of blue LED chip and QDs/hBN silicone gel were fabricated for long-term aging test under driving current of 200 mA. Their color coordinates were controlled at around (0.42, 0.17) for comparison. The QDs working temperature of QDs-LEDs and QDs/hBN-LEDs were measured as 125.8 and 102.5 °C (without metal-core printed circuit board (MCPCB)), respectively. The PL intensity of QDs was monitored every 24 h. Figure S4 (Supporting Information) shows the decay curves of these samples. It is seen that after 144 h of aging, 44% of the original PL intensity is still preserved for the QDs/hBN-LEDs, while the QDs-LEDs only retain 18% of the original PL intensity. From the illumination pattern in Figure S4 (Supporting Information), we can clearly observe the degradation of QDs-LEDs, which lost most of the red emission at the end of aging process, and its color coordinates shifted to (0.2021, 0.0599), while the color coordinates of QDs/hBN-LEDs only shifted to (0.2837, 0.1012). Therefore, the thermal-induced quenching of QDs can also be released by the QDs/hBN composites.

3. Conclusion

To cool the targeting QDs in phosphor-silicone matrix, we show an effective approach by incorporating QDs with thermally conductive hBN platelets. The optical and thermal performances of QDs/hBN-WLEDs were examined. Since the QDs and hBN platelets are electrostatically bonded, the heat generated by QDs can be effectively removed through the high thermal-conductive hBN channels. Overall, the thermal conductivity of optical converting layer was reinforced by 50% at 4.3% weight fraction of hBN. Compared with the QDs-WLEDs, the working temperature of QDs/hBN-WLEDs was reduced by 22.7 °C at 300 mA, while the luminous efficiency and color rendering index can be maintained as high as 108.5 lm W^{-1}, Ra > 95 and R9 > 90. The present strategy can improve heat dissipation of QDs without sacrificing the optical performance. The proposed method aims at enhancing the heat removal for QDs inside the LED packaging, which may trigger the development of package-inside thermal management (PITM) with practical and effective demonstrations.

4. Experimental Section

Preparation of QDs/hBN Composites: Highly luminescent red-emissive CdSe/ZnS core/shell QDs were provided by Poly OptoElectronics Co., Ltd. with some customization. It has been demonstrated that adding red QDs with peak wavelength of 626 nm into conventional phosphor-converted WLEDs could improve their color rendering index significantly.[10,28] Therefore, in this work, the QDs' peak wavelength was controlled to be around 626 nm by tuning the molar concentration of core and shell precursors. The QDs were precoated with cationic surface ligand (containing Cd^{2+} cation) before utilization.[29] hBN platelets with an average diameter of 12 µm were provided by Momentive. First, aqueous hBN solutions were prepared at a concentration of 1 g L^{-1} by sonication-assisted hydrolysis[30] under a bath sonicator for 8 h. These hydroxyl-functional hBN platelets presented negative surface charge due to the existence of hydroxyl groups. The resulting slurry was centrifuged at 6000 rpm for 5 min, and the hBN platelets were collected and dried in a vacuum oven under 80 for 12 h. Then, 1 g of the as-prepared hBN platelets was suspended in 10 mL of chloroform. Under magnetic stirring, 0.5 mL of QDs-chloroform solution (contains 5 mg QDs) was added dropwise. The zeta-potential measurements determined that the mean zeta-potential of QDs solution was positive (26.3 mV), while that of the hydroxyl-functional hBN was negative (–31.6 mV). Thus, the QDs nanoparticles attached to the surface of the platelets through the electrostatic interaction between the positively charged nanoparticles and negatively charged platelets.[31] The suspension was incubated for 1 h to coat the platelets with all the QDs nanoparticles. After that, the suspension was maintained at 60 °C until all the solvent was evaporated. The final QDs/hBN composites were obtained by a further drying process in vacuum oven at 50 °C.

Preparation of QDs- and QDs/hBN-WLEDs: Blue InGaN LED chip with peak wavelength of 455 nm and yellow-greenish YAG: Ce phosphor with peak wavelength of 538 nm were used. As displayed in Figure 1, for the preparation of QDs/hBN-WLEDs, 0.1 g of phosphor, 0.05 g of QDs/hBN composites, and 1 g of silicone gel (Dow corning OE 6550) were mixed and stirred for 20 min to be dispersed uniformly. Bubbles introduced during the stirring process were removed by applying alternating cycles

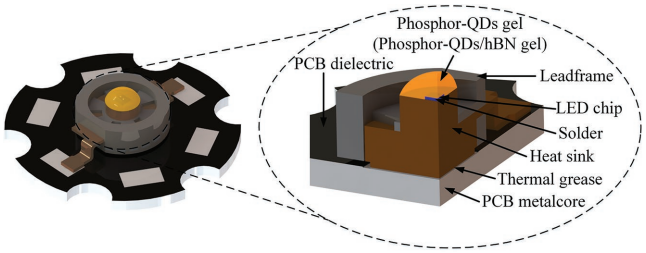

Figure 8. Structure schematics of a) QDs/hBN-WLEDs and b) QDs-WLEDs. (c–e) shows the heat power measuring process of LED chip, QDs/hBN-phosphor layer, and QDs-phosphor layer, respectively.

of vacuum. Then the mixed gel was coated onto the surface of LED chip, followed by a curing process in vacuum oven at 150 °C for 1 h. For comparative purposes, the QDs-WLEDs without hBN platelets were also prepared. First, 70 µL of QDs-chloroform solution and 0.12 g of phosphor were mixed with 1 g of silicone. Then the mixture was heated at 60 °C to remove the chloroform completely. Finally the mixture was coated onto the LED chip and cured. It is noted that these WLEDs were fabricated to have similar spectral power distribution, so that their thermal performances can be evaluated under the same optical conditions. Since the existence of hBN changes the light transmission/scattering situation. Therefore, the QDs' weight ratio for QDs/hBN-WLEDs and QDs-WLEDs to achieve the same spectral power distribution are different.

Measurement of Heat Generation: Since it is rather difficult to measure the temperature of the nanoscale QDs by experiments, it was prefered to examine the cooling performance of QDs/hBN- and QDs-WLEDs by finite element thermal simulation, and the heat generated by LED chip, QDs/hBN-phosphor silicone layer, and QDs-phosphor silicone layer were first measured by an integrating sphere system (ATA-1000, EVERFINE Inc.). The heat generation was calculated according to the optical energy loss within the corresponding layer. **Figure 8** illustrates the measuring process. Briefly, the energy loss of LED chip is calculated by the difference of input electrical power and output optical power of LED module with only silicone gel (Figure 8c); the energy loss of QDs/hBN-phosphor silicone layer is calculated by the difference of output optical power of LED module with only silicone gel and output optical power of LED module with QDs/hBN phosphor gel (Figure 8d); the energy loss of QDs-phosphor silicone layer is calculated by the difference of output optical power of LED module with only silicone gel and output optical power of LED module with QDs-phosphor gel (Figure 8e). The heat power of each layer is calculated as follows[32]

$$P_{\text{heat-chip}} = P_{\text{el}} - P_{\text{op,ref}} \quad (1)$$

$$P_{\text{QDs/hBN-phosphor}} = P_{\text{op,ref}} - P_{\text{op-1}} \quad (2)$$

$$P_{\text{QDs-phosphor}} = P_{\text{op,ref}} - P_{\text{op-2}} \quad (3)$$

where P_{el} is the input electrical power of WLEDs package, $P_{\text{op-1}}$ is the optical power from QDs/hBN-WLEDs, and $P_{\text{op-2}}$ is the optical power from QDs-WLEDs.

Thermal Simulation Setup: Before conducting the thermal simulations, the corresponding physical models of QDs/hBN- and QDs-WLEDs were built, as shown in **Figure 9**. The WLEDs were mounted onto a MCPCB by thermal grease for electrical connection and heat dissipation.

The thermal conductivity of phosphor-QDs gel and phosphor-QDs/hBN gel were calculated by $\kappa = \alpha C_p \rho$, where α, C_p, and ρ are thermal diffusivity, heat capacity, and density of the gel, respectively. In the thermal simulation, only a quarter of the WLEDs model was simulated due to its symmetry. The boundary conditions of the model were set as follows: the ambient temperature was fixed at 25 °C; natural convection occurred at the bottom surface of the PCB with a heat transfer coefficient of 10 W $(m^2\ K)^{-1}$, and other surfaces are cooled by natural convection with a heat transfer coefficient of 8 W $(m^2\ K)^{-1}$. All the boundary conditions are similar as those in.[32]

Measurement and Characterization: α was measured by a laser flash method using a Netzsch LFA 457. The geometry of the tested sample was a cylinder with diameter of 10 mm and thickness of around 1 mm. Before the test, a thin graphite film was applied on the composite surfaces to increase the energy absorption and the emittance of the surfaces. During the test, heat was propagated from the bottom to the top surface of the sample. C_p was determined by Perkin Elmer Diamond differential scanning calorimetry, and ρ was calculated from the weight fractions of the composite.

The PL spectra and absolute PLQY of the QDs solution and QDs/hBN platelets were measured by a Hamamatsu Quantaurus-QY under the excitation of 365 nm xenon lamp. The surface charge of the QDs and QDs/hBN solution was measured by using a Zeta-Potential Analyzer (Brookhaven BI-200SM). The TRPL measurements were carried out in air by an Edinburgh FLS 980 Fluorescence Spectrometers

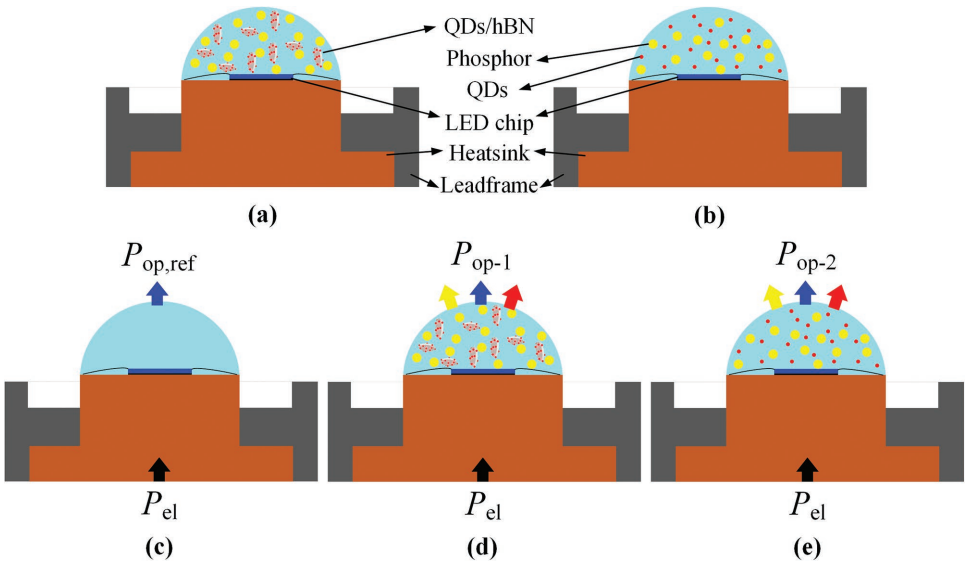

Figure 9. a–e) Physical model of the as-fabricated QDs/hBN- and QDs-WLEDs.

at a pulse excitation wavelength of 365 nm. TEM images of CdSe/ZnS core–shell QDs were done on a FEI Tecnai G2 F30 transmission electron microscope operating at an acceleration voltage of 300 kV. HAADF-STEM and EDS mapping images were acquired by a FEI Talos F200X transmission electron microscope operating at 300 kV. SEM and EDS mapping images were measured by a FEI Nova NanoSEM 450 at 15 kV. Brightness data were measured by an EVERFINE SRC-200M luminance meter. The surface temperature distributions of the WLEDs were obtained by an FLIR SC620 infrared thermal imager.

Supporting Information

Supporting Information is available from the Wiley Online Library or from the author.

Acknowledgements

This work was supported by National Natural Science Foundation of China (NFSC) (Nos. 51625601, 61604135, 51402148, and 51606074), National Key R&D Program of China (Nos. 2016YFB0100901 and 2016YFB0400804), Shenzhen Innovation Project (Nos. KC2014JSQN0011A and KQCX20140522151322950), the Ministry of Science and Technology of the People's Republic of China (No. 2017YFE0100600), and the Graduates' Innovation Fund, Huazhong University of Science and Technology (No. 5003120016). B.X. would like to acknowledge the technical support by Dr. Genrong Shao from Poly OptoElectronics Co., Ltd.

Conflict of Interest

The authors declare no conflict of interest.

Keywords

heat dissipation, light-emitting diodes, quantum dots, thermal conductivity

Received: February 23, 2018
Revised: April 18, 2018
Published online: June 4, 2018

[1] S. Pimputkar, J. S. Speck, S. P. DenBaars, S. Nakamura, *Nat. Photonics* **2009**, *3*, 180.
[2] X. Luo, R. Hu, S. Liu, K. Wang, *Prog. Energy Combust. Sci.* **2016**, *56*, 1.
[3] H. S. Jang, D. Y. Jeon, *Opt. Lett.* **2007**, *32*, 3444.
[4] X. Li, Y. Wu, S. Zhang, B. Cai, Y. Gu, J. Song, H. Zeng, *Adv. Funct. Mater.* **2016**, *26*, 2435.
[5] B. Xie, R. Hu, X. Luo, *J. Electron. Packag.* **2016**, *138*, 020803.
[6] K.-S. Cho, E. K. Lee, W.-J. Joo, E. Jang, T.-H. Kim, S. J. Lee, S.-J. Kwon, J. Y. Han, B.-K. Kim, B. L. Choi, J. M. Kim, *Nat. Photonics* **2009**, *3*, 341.
[7] R. Zhu, Z. Luo, H. Chen, Y. Dong, S.-T. Wu, *Opt. Express* **2015**, *23*, 23680.
[8] H. Chen, J. He, S.-T. Wu, *IEEE J. Quantum Electron* **2017**, *23*, 1900611.
[9] W. Chen, K. Wang, J. Hao, D. Wu, J. Qin, D. Dong, J. Deng, Y. Li, Y. Chen, W. Cao, *Nanophotonics* **2016**, *5*, 565.
[10] B. Xie, J. Zhang, W. Chen, J. Hao, Y. Cheng, R. Hu, D. Wu, K. Wang, X. Luo, *Nanotechnology* **2017**, *28*, 425204.
[11] N. Tomczak, D. Janczewski, M. Y. Han, G. J. Vancso, *Prog. Polym. Sci.* **2009**, *34*, 393.
[12] S. Kim, T. Kim, M. Kang, S. K. Kwak, T. W. Yoo, L. S. Park, I. Yang, S. Hwang, J. E. Lee, S. K. Kim, S.-W. Kim, *J. Am. Chem. Soc.* **2012**, *134*, 3804.
[13] Z. Li, W. Yao, L. Kong, Y. Zhao, L. Li, *J. Am. Chem. Soc.* **2015**, *137*, 12430.
[14] H.-C. Wang, S.-Y. Lin, A.-C. Tang, B. P. Singh, H.-C. Tong, C.-Y. Chen, Y.-C. Lee, T.-L. Tsai, R.-S. Liu, *Angew. Chem., Int. Ed.* **2016**, *55*, 7924.
[15] C. Sun, Y. Zhang, C. Ruan, C. Yin, X. Wang, Y. Wang, W. W. Yu, *Adv. Mater.* **2016**, *28*, 10088.
[16] Z. Li, L. Kong, S. Huang, L. Li, *Angew. Chem., Int. Ed.* **2017**, *56*, 8134.
[17] G. Lian, C.-C. Tuan, L. Li, S. Jiao, Q. Wang, K.-S. Moon, D. Cui, C.-P. Wong, *Chem. Mater.* **2016**, *28*, 6096.
[18] M. Wang, H. Chen, W. Lin, Z. Li, Q. Li, M. Chen, F. Meng, Y. Xing, Y. Yao, C.-P. Wong, Q. Li, *ACS Appl. Mater. Interfaces* **2014**, *6*, 539.
[19] V. Goyal, A. A. Balandin, *Appl. Phys. Lett.* **2012**, *100*, 073113.
[20] M. Poostforush, H. Azizi, *Express Polym. Lett.* **2014**, *8*, 293.
[21] T. Patel, S. Suin, D. Bhattacharya, B. B. Khatua, *Polym.–Plast. Technol.* **2013**, *52*, 1557.
[22] C. Yuan, B. Duan, L. Li, B. Xie, M. Huang, X. Luo, *ACS Appl. Mater. Interfaces* **2015**, *7*, 13000.
[23] W.-L. Song, P. Wang, L. Cao, A. Anderson, M. J. Meziani, A. J. Farr, Y.-P. Sun, *Angew. Chem., Int. Ed.* **2012**, *51*, 6498.
[24] Z. Lin, Y. Liu, S. Raghavan, K.-S. Moon, S. K. Sitaraman, C.-P. Wong, *ACS Appl. Mater. Interfaces* **2013**, *5*, 7633.
[25] R. Liang, J. Dai, L. Ye, L. Xu, Y. Peng, S. Wang, J. Chen, H. Long, C. Chen, *ACS Omega* **2017**, *2*, 5005.
[26] R. Hu, H. Zheng, J. Hu, X. Luo, *J. Disp. Technol.* **2013**, *9*, 447.
[27] L. Orloff, J. De Ris, G. H. Markstein, *Proc. Combust. Inst.* **1975**, *15*, 183.
[28] B. Xie, W. Chen, J. Hao, D. Wu, X. Yu, Y. Chen, R. Hu, K. Wang, X. Luo, *Opt. Express* **2016**, *24*, A1560.
[29] J. M. Luther, J. M. Pietryga, *ACS Nano* **2013**, *7*, 1845.
[30] Y. Lin, T. V. Williams, T.-B. Xu, W. Cao, H. E. Elsayed-Ali, *J. Phys. Chem. C* **2011**, *115*, 2679.
[31] R. M. Erb, R. Libanori, N. Rothfuchs, A. R. Studart, *Science* **2012**, *335*, 199.
[32] R. Hu, X. Luo, H. Zheng, *Jpn. J. Appl. Phys.* **2012**, *51*, 09MK05.